BIOCHEMISTRY
including biophysical chemistry & molecular biology

Article

pubs.acs.org/biochemistry

Structure–Function Studies of Hydrophobic Residues That Clamp a Basic Glutamate Side Chain during Catalysis by Triosephosphate Isomerase

John P. Richard,[*,†] Tina L. Amyes,[†] M. Merced Malabanan,[†] Xiang Zhai,[†] Kalvin J. Kim,[†] Christopher J. Reinhardt,[†] Rik K. Wierenga,[‡] Eric J. Drake,[§,∥] and Andrew M. Gulick[§,∥]

[†]Department of Chemistry, University at Buffalo, State University of New York, Buffalo, New York 14260, United States
[‡]Department of Biochemistry and Biocenter, University of Oulu, P.O. Box 3000, FIN-90014 Oulu, Finland
[§]Hauptman-Woodward Institute, 700 Ellicott Street, Buffalo, New York 14203, United States
[∥]Department of Structural Biology, University at Buffalo, State University of New York, Buffalo, New York 14203, United States

Supporting Information

ABSTRACT: Kinetic parameters are reported for the reactions of whole substrates (k_{cat}/K_m, M^{-1} s^{-1}) (*R*)-glyceraldehyde 3-phosphate (GAP) and dihydroxyacetone phosphate (DHAP) and for the substrate pieces [$(k_{cat}/K_m)_{E\cdot HP_i}/K_d$, M^{-2} s^{-1}] glycolaldehyde (GA) and phosphite dianion (HP_i) catalyzed by the I172A/L232A mutant of triosephosphate isomerase from *Trypanosoma brucei brucei* (*Tbb*TIM). A comparison with the corresponding parameters for wild-type, I172A, and L232A *Tbb*TIM-catalyzed reactions shows that the effect of I172A and L232A mutations on $\Delta G^{\ddagger}$ for the wild-type *Tbb*TIM-catalyzed reactions of the substrate pieces is nearly the same as the effect of the same mutations on *Tbb*TIM previously mutated at the second side chain. This provides strong evidence that mutation of the first hydrophobic side chain does not affect the functioning of the second side chain in catalysis of the reactions of the substrate pieces. By contrast, the effects of I172A and L232A mutations on $\Delta G^{\ddagger}$ for wild-type *Tbb*TIM-catalyzed reactions of the whole substrate are different from the effect of the same mutations on *Tbb*TIM previously mutated at the second side chain. This is due to the change in the rate-determining step that determines the barrier to the isomerization reaction. X-ray crystal structures are reported for I172A, L232A, and I172A/L232A TIMs and for the complexes of these mutants to the intermediate analogue phosphoglycolate (PGA). The structures of the PGA complexes with wild-type and mutant enzymes are nearly superimposable, except that the space opened by replacement of the hydrophobic side chain is occupied by a water molecule that lies ~3.5 Å from the basic side chain of Glu167. The new water at I172A mutant *Tbb*TIM provides a simple rationalization for the increase in the activation barrier $\Delta G^{\ddagger}$ observed for mutant enzyme-catalyzed reactions of the whole substrate and substrate pieces. By contrast, the new water at the L232A mutant does not predict the decrease in $\Delta G^{\ddagger}$ observed for the mutant enzyme-catalyzed reactions of the substrate piece GA.

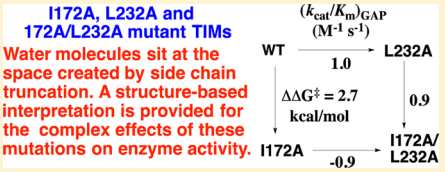

X-ray crystal structures of enzymes show the positioning of amino acid side chains that participate in catalysis. This is a key piece in the puzzle of experimental results, which enzymologists must assemble in rationalizing the rate enhancements for enzymatic reactions. We are working to assemble the puzzle of results from studies of the triosephosphate isomerase-catalyzed (TIM) conversion of (*R*)-glyceraldehyde 3-phosphate (GAP) to dihydroxyacetone phosphate (DHAP) through enzyme-bound *cis*-enediolate reaction intermediates (Scheme 1).[1−6]

It has been more than 20 years since the conclusion, from the examination of X-ray crystal structures of TIM and the effect of site-directed mutations on enzyme structure, that the TIM-catalyzed proton transfer reactions at carbon and oxygen are mediated by the side chains of Glu165/167[a,7−10] and His95,[11−13] respectively, by a mechanism similar to that for catalysis of non-enzymatic isomerization in water.[2,14] This work resolves essential questions about the enzymatic reaction mechanism but does not provide an explanation for the enzymatic rate enhancement. The answer to the second question requires a detailed consideration for why the functional groups at TIM provide a level of stabilization of the isomerization transition states greater than that observed for catalysis by the same functional groups in water.[2,14] This ignorance causes problems for protein engineers, who are able to insert catalytic side chains at protein clefts or pockets but who lack an understanding of the properties of the local active site environment that must be mimicked to obtain TIM-like activity for a protein catalyst.

The active site of TIM represents the end product of natural selection of proteins that satisfy the imperatives for catalysis of deprotonation of weakly acidic α-carbonyl carbon.[15−17] The strongest imperative is to reduce the large thermodynamic barrier for the transfer of a proton from the α-carbonyl carbon of DHAP and GAP to the side chain of Glu165/167,[15,18,19] by increasing the side

Received: April 4, 2016
Revised: May 2, 2016
Published: May 5, 2016

DOI: 10.1021/acs.biochem.6b00311
Biochemistry 2016, 55, 3036−3047

Scheme 1

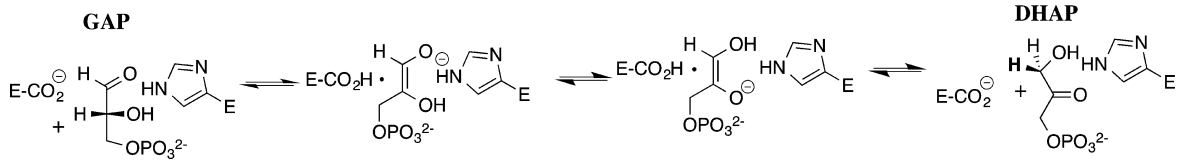

chain basicity relative to that for the carbanion intermediate. This change in driving force is effected during a ligand-driven conformational change, which converts the open form of unliganded TIM, with a side chain pK_a of ≈4, to an active caged complex with ligands (Figure 1A),[20,21] for which a side chain

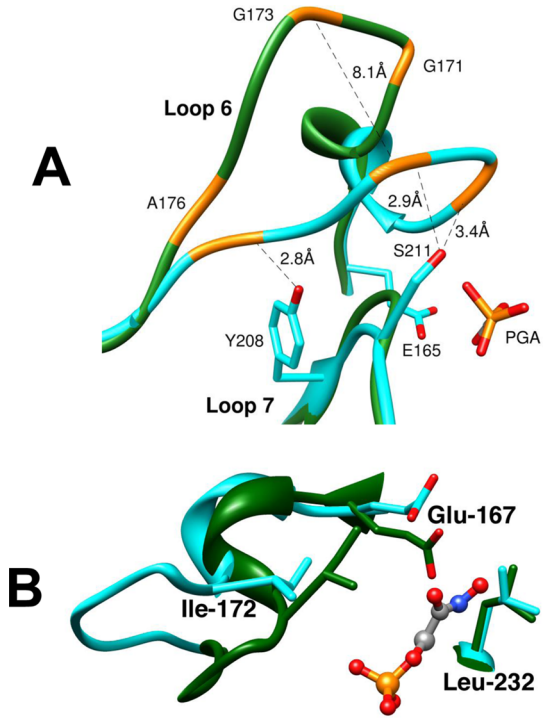

Figure 1. (A) Structural representations of the open unliganded form of yeast TIM (PDB entry 1YPI) and the closed complex with PGA, an analogue of the enediolate reaction intermediate (PDB entry 2YPI). These representations show the 8.1 Å displacement of Gly173 that occurs during loop closure and the intraloop hydrogen bonds between the hydroxyl of Y208 (loop 7) and the amide of A176 (loop 6) and between the hydroxyl of S211 and the carbonyl oxygen and amide nitrogen from A169 and G173, respectively. (B) Structural representations of the active sites of unliganded open (cyan, PDB entry 5TIM) and the PGH-liganded closed (green, PDB entry 1TRD) forms of *Tbb*TIM. Closure of loop 6 over the ligand results in movement of the side chain of Ile172 toward the carboxylate side chain of the catalytic base Glu167 and movement of Glu167 toward the side chain of Leu232, which maintains a nearly fixed position. Reprinted with permission from ref 28. Copyright 2012 American Chemical Society.

pK_a of >9.3 has been determined for the complex with phosphoglycolate.[22,23] This cage forms by closure of loop 6 (168-PVWAIGTGKTA) over the ligand and is stabilized by interactions between backbone amides from loop 6 and the side chains of Tyr208/Try210 and Ser211/Ser213 from loop 7 (210-YGGS-213).[24−26] Cage formation is accompanied by (i) the folding of the hydrophobic side chain of Ile172 over the side chain of Glu167 (Figure 1B),[9] (ii) the movement of Glu167 toward the hydrophobic side chain of Leu232, and (iii) the displacement to solvent of four of six water molecules that lie within 6 Å of the carboxylate side chain.[5,27] The result is to lock the carboxylate side chain in a hydrophobic clamp and enhance the side chain basicity toward deprotonation of the enzyme-bound substrate.[20]

We previously reported the preparation and kinetic parameters for I172A and L232A mutants of TIM from *Trypanosoma brucei brucei* (*Tbb*TIM).[28,29] The I172A mutation results in 100- and 200-fold decreases in the second-order rate constant $(k_{cat}/K_m)_{GAP}$ for catalysis of isomerization of GAP and the third-order rate constant $k_{cat}/K_{GA}K_{HP_i}$ for phosphite dianion (HPO_3^{2-}) activation of TIM, respectively, for catalysis of reactions of the truncated substrate glycolaldehyde (GA) in D_2O (Scheme 2).[28−31] These results show that the reactivity of

Scheme 2

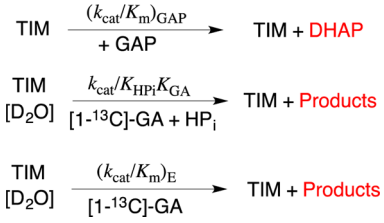

wild-type TIM toward deprotonation of carbon acid substrates is enhanced by interactions with the hydrophobic side chain of Ile172 (Figure 1B). The I172A mutation of *Tbb*TIM results in a ≈2-unit decrease, from >9.3 to 7.7, in the pK_a of the carboxylic acid side chain of Glu167 that is hydrogen-bonded to the enediolate analogue phosphoglycolate (PGA). This links the enhancement of the chemical reactivity of wild-type TIM to an enhancement of the basicity of the carboxylate side chain from interactions with the side chain of Ile172.[20]

By contrast, the L232A mutation results in a small 6-fold decrease in the second-order rate constant k_{cat}/K_m for catalysis of isomerization of GAP; in startling 25- and 20-fold increases in $k_{cat}/K_{GA}K_{HP_i}$ and $(k_{cat}/K_m)_E$, respectively, for TIM-catalyzed reactions of GA (Scheme 2); and in an increase in the enzyme affinity for binding PGA.[29] These data are consistent with the conclusion that the L232A mutation results in an ≈1.7 kcal/mol stabilization of a catalytically active loop-closed form of TIM relative to an inactive open form, and that this results in an ∼20-fold increase in the fraction of TIM present in an active form. We report here the preparation of I172A/L232A *Tbb*TIM and kinetic parameters for mutant enzyme-catalyzed reactions of GAP and the substrate pieces GA and HPO_3^{2-}. The double mutation results in complex changes in the kinetic parameters for the reactions catalyzed by the I172A and L232A mutants, which are consistent with our proposed roles for these side chains in the catalysis of deprotonation of GAP and DHAP.[28]

Our interpretation of kinetic data for the I172A and L232A mutants relied on X-ray crystal structures for wild-type *Tbb*TIM, and the assumption that these mutations cause only small changes in the structure of TIM. We now report X-ray crystal structures

DOI: 10.1021/acs.biochem.6b00311
Biochemistry 2016, 55, 3036−3047

for unliganded I172A, L232A, and I172A/L232A TIMs, and for complexes of the mutant enzymes with PGA. These crystal structures confirm the assumption that mutations I172A and L232A do not cause significant changes in the position of catalytic side chains at the enzyme active site.

EXPERIMENTAL PROCEDURES

The source of the materials used in this study and the methods for the preparation of solutions were provided in earlier publications.[20,28,32] The I172A/L232A double mutant of *Tbb*TIM was prepared starting from the plasmid bearing the L232A mutation.[28] Site-directed mutagenesis to introduce the I172A mutation was conducted using *Pfu* Ultrahigh Fidelity DNA Polymerase following the Stratagene protocol. The primer that was used to introduce the I172A mutation was 5′-CCC-GTT-TGG-GCC-GCG-GGT-ACC-GGC-AAG-GTG-GCG-ACA-CC-3′, in which the altered codon is underlined. The presence of the gene for the I172A/L232A double mutant of *Tbb*TIM was verified by DNA sequencing at the Roswell Park Cancer Institute (Buffalo, NY). 2-Phosphoglycolate (PGA) was prepared as described previously.[33]

I172A/L232A *Tbb*TIM was expressed in *Escherichia coli* BL21 pLysS grown in LB medium at 18 °C, and the protein was purified by ammonium sulfate precipitation followed by gradient elution on a CM Sepharose cation exchanger.[34] The enzyme obtained from this column was judged to be homogeneous by gel electrophoresis. The concentration of the protein was determined from the absorbance at 280 nm and the extinction coefficient of 3.5×10^4 M^{-1} cm^{-1} calculated using the ProtParam tool available on the Expasy server.[35,36]

Enzyme Kinetic Parameters. All enzyme assays of whole substrates DHAP and GAP were conducted at 25 °C, and pH 7.5 was maintained with 30 mM triethanolamine buffer using published procedures.[28,29,32] The values of k_{cat} and K_m for mutant *Tbb*TIM-catalyzed isomerization of GAP were determined from the fit to the Michaelis−Menten equation of initial reaction velocities (v_i) determined at varying GAP concentrations. The arsenate dianion used with the glyceraldehyde 3-phosphate dehydrogenase coupling enzyme in the assay for TIM-catalyzed isomerization of DHAP is a competitive inhibitor of wild-type *Tbb*TIM.[37] Values for k_{cat}, K_m, and K_i for the I172A/L232A mutant-catalyzed isomerization of DHAP were determined from the nonlinear least-squares fit to eq 1 of initial velocities determined at varying concentrations of arsenate dianion (5, 10, and 15 mM) and DHAP (eight concentrations between 0.12 and 8 mM). This fitting procedure gave a K_i value of 0.93 mM for inhibition of the mutant enzyme by arsenate dianion. Values of K_i for competitive inhibition of I172A/L232A TIM by PGA at pH 7.5 [I = 0.1 (NaCl)] were determined by examining the effect of increasing concentrations of GAP on the initial velocity of TIM-catalyzed isomerization in the presence of two different fixed concentrations of PGA. The concentration of the glycerol-3-phosphate dehydrogenase coupling enzyme was increased, as needed in these assays to overcome inhibition by PGA.

$$\frac{v_i}{[E]} = \frac{k_{cat}[DHAP]}{K_m(1 + [HOAsO_3^{2-}]/K_i) + [DHAP]} \quad (1)$$

Reactions of [1-^{13}C]-GA in D_2O. The products of I172A/L232A *Tbb*TIM-catalyzed reactions of [1-^{13}C]-GA in the presence or absence of HPO_3^{2-} in D_2O at 25 °C were determined by ^{1}H NMR analyses as described previously.[30] The NMR spectra were recorded in D_2O at 25 °C using a Varian Unity Inova 500 spectrometer that was shimmed to give a line width of ≤0.5 Hz for the most downfield peak of the double triplet due to the C-1 proton of the hydrate of [1-^{13}C]-GA.[30] Spectra (16 transients) were obtained using a sweep width of 6000 Hz, a pulse angle of 90°, and an acquisition time of 6 s. A total relaxation delay of 120 s (>8T_1) between transients was used to ensure that accurate integrals were obtained for the protons of interest.[18,38,39] Baselines were subjected to a first-order drift correction before determination of integrated peak areas. Chemical shifts are reported relative to that for HOD at 4.67 ppm.

The mutant enzyme was exhaustively dialyzed at 7 °C against 30 mM imidazole (20% free base, pD 7.0) in D_2O at an ionic strength of either 0.024 or 0.1 (NaCl). The reactions in the absence of phosphite were initiated by adding enzyme to give a solution that contained 20 mM [1-^{13}C]-GA, 20 mM imidazole [20% free base, pD 7.0, I = 0.1 (NaCl)], and 220 or 350 μM I172A/L232A *Tbb*TIM in a volume of 850 μL. The reactions in the presence of HPO_3^{2-} were initiated by adding enzyme to give a solution that contained 20 mM [1-^{13}C]-GA, 20 mM imidazole (20% free base, pD 7.0), 1−40 mM HPO_3^{2-} (50% dianion, pD 7.0), and 190 μM I172A/L232A *Tbb*TIM in a volume of 850 μL (I = 0.1). In every case, 750 μL of the reaction mixture was transferred to an NMR tube, the ^{1}H NMR spectrum was recorded immediately, and spectra were then recorded at regular intervals. The remaining solution was incubated at 25 °C and the enzyme assayed for activity toward isomerization of GAP. No significant loss of enzyme activity was observed during any of these reactions. At the end of each NMR experiment, the protein was removed by ultrafiltration and the pD of the solution was determined. There was no significant change (<0.10 unit) in pD during these reactions.

The observed ^{1}H NMR peak areas for the reaction products were normalized, as described in previous work, using the signal due to the C-4 and C-5 protons of imidazole or the upfield peak of the doublet due to the P−H proton of HPO_3^{2-} as an internal standard.[30] The fraction of the substrate [1-^{13}C]-GA remaining and the fractional yields of the identifiable reaction products [2-^{13}C]-GA, [2-^{13}C,2-^{2}H]-GA, [1-^{13}C,2-^{2}H]-GA, and [1-^{13}C,2,2-di-^{2}H]-GA (Chart 1) were determined, as described previously, from the integrated areas of the relevant ^{1}H NMR signals for these compounds.[30] The disappearance of 30−70% [1-^{13}C]-GA was monitored, and product yields were determined over the first ∼20% of the reaction.

Chart 1

[1-^{13}C]-GA [2-^{13}C]-GA [2-^{13}C, 2-^{2}H]-GA [1-^{13}C, 2-^{2}H]-GA [1-^{13}C, 2,2-di-^{2}H]-GA

DOI: 10.1021/acs.biochem.6b00311
Biochemistry 2016, 55, 3036−3047

Observed first-order rate constants, k_{obs} (s^{-1}), for the reactions of [1-^{13}C]-GA were determined from the slopes of linear semilogarithmic plots of reaction progress versus time (eq 2), where f_S is the fraction of [1-^{13}C]-GA remaining at time t. Observed second-order rate constants, $(k_{cat}/K_m)_{obs}$ (M^{-1} s^{-1}), for the TIM-catalyzed reaction of [1-^{13}C]-GA were determined from the values of k_{obs} using eq 3, where f_{hyd} (=0.94) is the fraction of [1-^{13}C]-GA present as the hydrate.[31]

$$\ln f_S = -k_{obs}t \quad (2)$$

$$(k_{cat}/K_m)_{obs} = \frac{k_{obs}}{(1 - f_{hyd})[TIM]} \quad (3)$$

Protein Crystallization. Mutant TIMs, purified as described here or in previous work,[28] were dialyzed against a crystallization buffer consisting of 10 mM Tris-HCl at pH 8.0. The crystallization conditions for all mutants (7−10 mg/mL, 0.3−0.4 mM TIM subunits) were optimized from leads first identified in a sparse matrix screen. For drops containing the PGA ligand, the protein was incubated for 45 min on ice in the presence of a 1.2-fold subunit molar excess of PGA (0.36−0.48 mM) before being set up for crystallization. Crystals were mounted in nylon loops and cryoprotected by being passed through three precipitant solutions containing increasing amounts of 2-methyl-2,4-pentanediol (MPD) (8, 16, and 24%) for approximately 30 s each and frozen in liquid nitrogen.

Data Collection and Crystallographic Refinement. Data were collected either on a home source or at beamline 7-1 at the Stanford Synchrotron Radiation Lightsource (SSRL, Menlo Park, CA). Data processing was conducted using iMOSFLM[40] or HKL2000.[41] All models were solved using MOLREP[42] from the CCP4 data suite. PDB entry 3TIM was used as a search model. Waters were placed into spherical density peaks in both the $2F_o - F_c$ and $F_o - F_c$ difference maps, at positions where reasonable hydrogen bonding geometry to neighboring heteroatoms could be identified. The resulting output model was used for continued cycles of manual model building with COOT,[43] REFMAC5,[44] and PHENIX.[45] The X-ray crystal structures have been deposited in the Protein Data Bank (PDB entries 5I3F for the I172A mutant, 5I3G for the I172A/L232A mutant, 5I3H for the complex of PGA with the I172A/L232A mutant, 5I3I for the complex of PGA with the I172A mutant, 5I3J for the L232A mutant, and 5I3K for the complex of PGA with the L232A mutant).

RESULTS

Kinetic and Product Studies. Table 1 compares the kinetic parameters for isomerization of GAP and DHAP at pH 7.5 (30 mM TEA) and 25 °C [I = 0.1 (NaCl)] catalyzed by the I172A/L232A *Tbb*TIM with kinetic parameters for the wild-type, I172A, and L232A TIM-catalyzed reactions determined previously.[28,29] The competitive inhibition of the I172A/L232A mutant by PGA at pH 7.5 (30 mM TEA) and 25 °C was examined at several concentrations of GAP, for two different fixed PGA concentrations (0.26 and 0.64 mM). The K_i value of $(1.2 \pm 0.15) \times 10^{-4}$ M for inhibition was obtained from the nonlinear least-squares fit of the initial velocity data to eq 4 and using the value of K_m from Table 1. By comparison, K_i values of $(6.9 \pm 0.7) \times 10^{-5}$ (pH 7.5), $(2.6 \pm 0.2) \times 10^{-3}$ (pH 7.5), and $(1.2 \pm 0.1) \times 10^{-5}$ M (pH 8.3) have been reported for inhibition of wild-type, I172A, and L232A TIMs, respectively, by PGA.[20]

$$\frac{v_i}{[E]} = \frac{k_{cat}[GAP]}{[GAP] + K_m(1 + [PGA]/K_i)} \quad (4)$$

The I172A/L232A *Tbb*TIM-catalyzed reactions of [1-^{13}C]-GA in D_2O at pD 7.0, 25 °C, and I = 0.1 were monitored by ^{1}H NMR spectroscopy.[30] The disappearance of [1-^{13}C]-GA was monitored for 40−70% of completion for the reactions in the presence of HPO_3^{2-}, but for only 20−25% of completion for the slower reaction in the absence of this dianion. The observed first-order rate constants, k_{obs}, and the second-order rate constants, $(k_{cat}/K_m)_{obs}$ (Table S1), for TIM-catalyzed reactions of [1-^{13}C]-GA were determined according to eqs 2 and 3, respectively, as described in Experimental Procedures.

The averages of the product yields, determined at four different times during the first 20−30% of the I172A/L232A mutant enzyme-catalyzed reaction of [1-^{13}C]-GA, are reported in Table S1. The mutant *Tbb*TIM-catalyzed reactions of [1-^{13}C]-GA in the presence of phosphite dianion are >4 times faster than the unactivated reactions (Table S1). No (<5%) dideuterium-labeled product [1-^{13}C,2,2-di-^{2}H]-GA from a nonspecific protein-catalyzed reaction (Scheme 3B)[30,32,46] was detected, so that the dominant reaction products are from the phosphite dianion-activated reactions of [1-^{13}C]-GA at the enzyme active site (Scheme 3A).[30]

The slow unactivated reaction of [1-^{13}C]-GA in the absence of phosphite dianion gives a 30% yield of [1-^{13}C,2,2-di-^{2}H]-GA from nonspecific protein-catalyzed reactions (Scheme 3B),[30,32,46] a 20% yield of [1-^{13}C,2-^{2}H]-GA, a 50% yield of unidentified reaction products, but no [2-^{13}C]-GA or [2-^{13}C,2-^{2}H]-GA from reactions at the enzyme active site (Scheme 3A).[30,32,46] The 20% yield of [1-^{13}C,2-^{2}H]-GA forms mainly by a nonspecific reaction (Scheme 3B), rather than from partitioning of the enzyme-bound enediolate intermediate (Scheme 3A), because this partitioning gives a 55/45 mixture of [1-^{13}C,2-^{2}H]-GA and [2-^{13}C,2-^{2}H]-GA for dianion-activated reaction, but no [2-^{13}C,2-^{2}H]-GA is observed from the unactivated reaction (Table S1). We conclude

Table 1. Kinetic Parameters for the Isomerization Reactions of GAP and DHAP Catalyzed by Wild-Type and Mutant Forms of *Tbb*TIM[a]

	GAP			DHAP		
*Tbb*TIM	k_{cat} (s^{-1})	K_m (M)	k_{cat}/K_m (M^{-1} s^{-1})[b]	k_{cat} (s^{-1})	K_m (M)	k_{cat}/K_m (M^{-1} s^{-1})
WT[c]	2100	2.5×10^{-4}	8.4×10^6 (2.1×10^8)	300	7.0×10^{-4}	4.3×10^5
I172A[d]	12	1.5×10^{-4}	8.0×10^4 (2.0×10^6)	17	3.7×10^{-3}	4.6×10^3
L232A[d]	220	1.4×10^{-4}	1.5×10^6 (3.8×10^7)	4.7	7.7×10^{-5}	6.1×10^4
I172A/L232A[e]	6.3	1.8×10^{-5}	3.5×10^5 (8.8×10^6)	1.1	6.2×10^{-5}	1.8×10^4

[a]Under standard assay conditions: 30 mM TEA, pH 7.5, and 25 °C [I = 0.1 (NaCl)]. In most cases, the variation in k_{cat} and K_m determined in different experiments is less than ±15%. [b]The values in parentheses are calculated for the reaction of the active carbonyl form of the substrate, which is present as 4% of the total substrate.[58,59] [c]Data from ref 32. [d]Data from ref 28. [e]This work.

DOI: 10.1021/acs.biochem.6b00311
Biochemistry 2016, 55, 3036−3047

Scheme 3

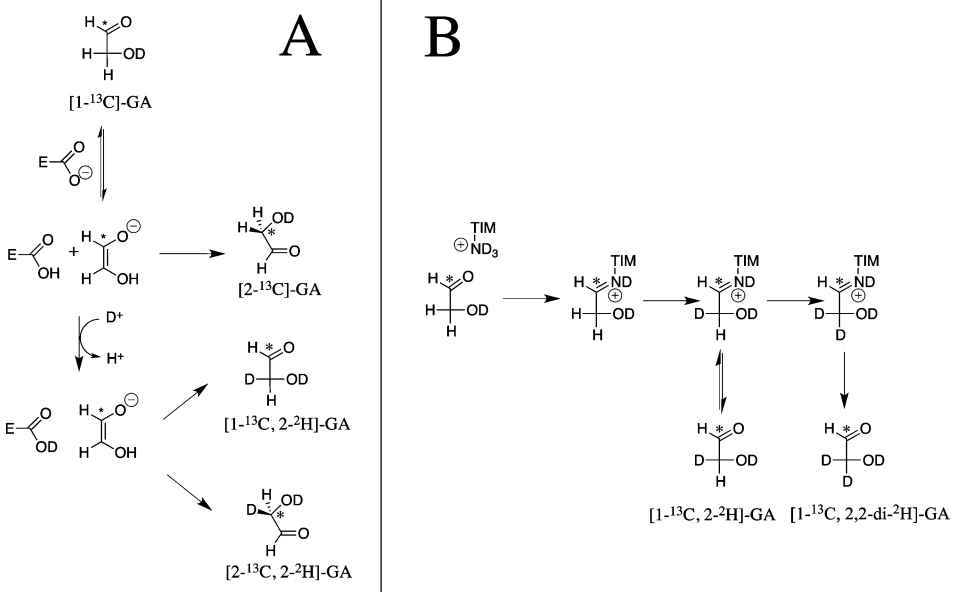

Scheme 4

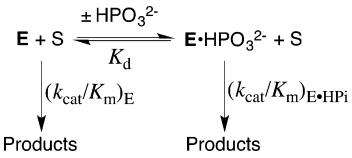

that [1-^{13}C,2,2-di-^{2}H]-GA and [1-^{13}C,2-^{2}H]-GA from the unactivated reaction form by nonspecific protein-catalyzed reactions (Scheme 3B), so that $(k_{cat}/K_m)_E \approx 0$ (Scheme 4) for reactions of [1-^{13}C]-GA at the enzyme active site.

Figure 2 shows the increase in $(k_{cat}/K_m)_{obs} - (k_{cat}/K_m)_o$ at increasing HPO_3^{2-} concentrations for I172A/L232A *Tbb*TIM-catalyzed reactions of [1-^{13}C]-GA in D_2O at pD 7.0 (25 °C, I = 0.1), where $(k_{cat}/K_m)_{obs}$ is the observed reaction rate constant

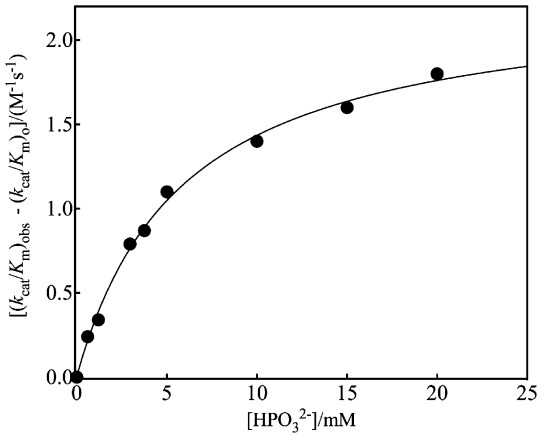

Figure 2. Dependence of the second-order rate constants $k_{cat}/K_m = (k_{cat}/K_m)_{obs} - (k_{cat}/K_m)_o$ for the I172A/L232A *Tbb*TIM-catalyzed turnover of the carbonyl form of [1-^{13}C]-GA in D_2O on the concentration of HPO_3^{2-} at pD 7.0 and 25 °C (I = 0.1). The data were fit to eq 5 derived for Scheme 4.

(Table S1) and $(k_{cat}/K_m)_o$ = 0.068 M^{-1} s^{-1} is the rate constant for the protein-catalyzed reaction (Scheme 3B) determined without HPO_3^{2-}. The data from Figure 2 were fit to eq 5, derived for Scheme 4, using $(k_{cat}/K_m)_E = 0$ (see above) to give the values of K_d and $(k_{cat}/K_m)_{E\cdot HP_i}$ reported in Table 2. Table 2 also reports kinetic parameters for the wild-type, I172A, and L232A enzyme-catalyzed reactions reported previously.[28,29,32]

$$\left(\frac{k_{cat}}{K_m}\right)_{obs} - \left(\frac{k_{cat}}{K_m}\right)_o = \left(\frac{[HPO_3^{2-}]}{K_d + [HPO_3^{2-}]}\right)\left(\frac{k_{cat}}{K_m}\right)_{E\cdot HP_i} \quad (5)$$

X-ray Crystallographic Analysis. To analyze the impact of the I172A and L232A mutations, we determined the crystal structures of both single-mutant enzymes and the I172A/L232A double-mutant enzymes in the presence and absence of the intermediate analogue PGA. Crystallization, diffraction, and refinement data are listed in Tables S2–S4, respectively, of the Supporting Information. The proteins crystallized in triclinic or monoclinic space groups with multiple chains present in the asymmetric unit. The structures were determined at resolutions ranging from 1.7 to 2.3 Å (Table S4).

The ligand-free form of TIM is "open", with the active site cavity exposed to solvent.[4,5,47] Structures of ligand-free mutant TIMs were compared with the structure of ligand-free wild-type *Tbb*TIM (PDB entry 5TIM, subunit A). In every case in which the disordered flexible loop 6 is excluded from the comparison, the superimposed structures of ligand-free wild-type and mutant TIMs show root-mean-square displacements of 0.2–0.4 Å for all protein Cα atoms. We conclude that I172A and L232A mutations result in minimal changes in the protein fold of the ligand-free enzyme.

Ligand binding is accompanied by a change in protein conformation to form the "closed" catalyst.[4,5,47] This involves a large movement of the initially disordered loop 6 to an ordered structure, where the loop sits over the substrate phosphodianion and traps the substrate at the active site.[24] Movement of loop 6 is accompanied by rotation of two peptide bonds at

DOI: 10.1021/acs.biochem.6b00311
Biochemistry 2016, 55, 3036–3047

Table 2. Kinetic Parameters (Scheme 4) for the Phosphite-Activated and Unactivated Reactions of [1-^{13}C]-GA Catalyzed by Wild-Type and Mutant Forms of *Tbb*TIM[a]

*Tbb*TIM	$(k_{cat}/K_m)_E$ (M^{-1} s^{-1})	$(k_{cat}/K_m)_{E\cdot HP_i}$ (M^{-1} s^{-1})	K_d (mM)	*x*-fold activation by phosphite dianion[b]	$(k_{cat}/K_m)_{E\cdot HP_i}/K_d$ (M^{-2} s^{-1})
WT[c]	0.07	64	19	900	3400
I172A[d]	<0.003	0.23	12	>77	20
L232A[d]	1.2	100	1.2	80	83000
I172A/L232A[e]	<0.003[f]	2.3 ± 0.1	5.9 ± 0.5	>315	390

[a]For reactions at pD 7.0 and I = 0.1 (NaCl). [b]The effect of TIM-bound phosphite dianion on the second-order rate constant for TIM-catalyzed reactions of GA, calculated as $[(k_{cat}/K_m)_{E\cdot HP_i}]/(k_{cat}/K_m)_E$. [c]Data from ref 32. [d]Data from ref 28. [e]From this work. The quoted error is the standard deviation for the fit of the data from Figure 2 to eq 5. [f]The smallest detectable rate constant for these experiments, estimated as described previously.[28]

loop 7, which swings the side chains of Tyr210 and Ser213 into a position to hydrogen bond with backbone amides of loop 6 (Figure 1A).[4,5,48] The subunits of the crystals of TIM, which were grown in the presence of PGA, are found in either the "open" or "closed" form depending upon whether a bound ligand is observed (Table S5). The subunits with PGA bound exist in the closed conformation, and the ligand-free subunits show loops 6 and 7 in the open conformation that is identical to ligand-free wild-type TIM.

The asymmetric unit of the complex of the I172A mutant contains a dimer pair, and all four subunit chains (A–D) show electron density for PGA. The liganded subunit A is used for comparisons with the structures of other TIM·PGA complexes. The asymmetric unit of L232A *Tbb*TIM grown in the presence of PGA also contains a dimer pair. The chains for subunits B and C in one dimer show good density for PGA, while subunits A and D for the second dimer show subunit D in a complex with PGA and ligand-free subunit A. The complex of PGA with subunit B is used for comparisons with the structures of other TIM·PGA complexes. The asymmetric unit of the crystalline I172A/L232A mutant grown in the presence of PGA shows one dimer per asymmetric unit. Subunit A is unliganded, and liganded subunit B is used in structural comparisons with other liganded TIMs.

The structures of the complexes of PGA with the subunits of mutant TIMs, noted above, were compared with the structure of wild-type *Tbb*TIM liganded to 2-phosphoglycerate (PDB entry 4TIM, subunit B). In each case, the superimposed structures of wild-type and mutant TIMs give root-mean-square displacements of 0.2–0.4 Å for all Cα atoms of the protein. We conclude that I172A and L232A mutations result in minimal changes in the overall protein fold of the liganded subunits chosen for this comparison. While subtle differences in the water structure exist at the exterior of the active site cavity, the new waters that replace the deleted side chains are the only changes in the interior of the active site. The active site X-ray crystal structures of the TIM subunits, noted above, that contain the PGA ligand were also compared with the atomic level resolution (0.83 Å) X-ray crystal structure of the complex of PGA with wild-type TIM from *Leishmania mexicana* (*Lm*TIM) (PDB entry 1N55).[9]

There is no evidence of half-site reactivity in the binding of ligands to TIM subunits in solution. We therefore expect that the occurrence, described above, of both open/unliganded and closed/liganded active sites within crystals grown in the presence of PGA reflects structural differences in the subunit chains. We are unable to provide a clear explanation for the preference of some subunits to adopt an open conformation. For example, careful analyses of loops at the subunits present in the open form provide no clear evidence of crystal contacts that stabilize the open enzyme.

DISCUSSION

Occam's razor was applied in earlier discussions of the effects of I172A and L232A mutations on kinetic parameters for TIM-catalyzed reactions of the whole substrate GAP and the substrate pieces GA and HPO_3^{2-}, which were interpreted by a minimal model that assumed these mutations do not significantly affect the protein structure.[28,29] We test this model in the experiments reported in this paper. The kinetic parameters for I172A/L232A *Tbb*TIM-catalyzed reactions of whole substrate GAP (Table 1) and the substrate pieces GA and HPO_3^{2-} (Table 2) were determined. These data allow a comparison of the effects of I172A and L232A mutations on the activation barriers ($\Delta G^{\ddagger}$) for wild-type *Tbb*TIM and the corresponding effects of the same mutations on $\Delta G^{\ddagger}$ for *Tbb*TIM previously mutated at the second site (Scheme 5).

Scheme 5. (A) Effect of I172A and L232A Mutations of *Tbb*TIM on the Activation Barrier ($\Delta G^{\ddagger}$) for the *Tbb*TIM-Catalyzed Reactions of the Substrate Pieces [1-^{13}C]-GA and HPO_3^{2-} (Scheme 4) and (B) Effect of I172A and L232A Mutations of *Tbb*TIM on the Activation Barrier ($\Delta G^{\ddagger}$) for the *Tbb*TIM-Catalyzed Reactions of the Whole Substrate GAP

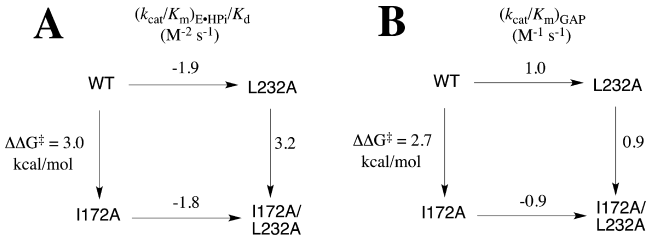

The I172A and L232A mutations of wild-type *Tbb*TIM result in a 3.0 kcal/mol destabilization and a startling 1.9 kcal/mol stabilization of the transition state, respectively, for the reaction of the substrate pieces (Scheme 5A).[29] The former effect on $\Delta G^{\ddagger}$ is associated with an ~2 unit decrease in the pK_a of the carboxylate side chain of I172A *Tbb*TIM compared with that of wild-type *Tbb*TIM,[20] while the latter effect was attributed to an ~20-fold increase in K_C for the thermodynamically unfavorable [$K_C \ll 1$ (Scheme 6)] enzyme conformational change, which is discussed in a later section.[28,29]

Scheme 5A shows that the I172A and L232A mutations in L232A and I172A *Tbb*TIM result in a 3.2 kcal/mol destabilization and a 1.8 kcal/mol stabilization of the transition states, respectively, for the reaction of the substrate pieces. These effects on $\Delta G^{\ddagger}$ are nearly the same as for the same point mutations at wild-type *Tbb*TIM. This result shows that the first I172A and L232A mutations do not affect the functioning of

DOI: 10.1021/acs.biochem.6b00311
Biochemistry 2016, 55, 3036–3047

Scheme 6

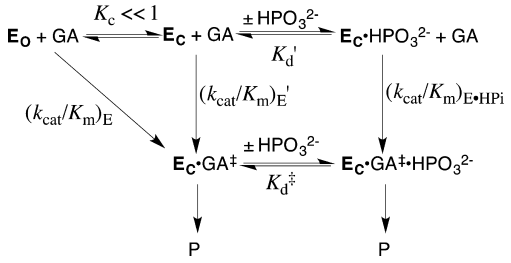

the remaining hydrophobic side chain. It is consistent with the conclusion that the effects of these initial mutations are localized to the specific interactions of the eliminated side chain and that there are no long-range effects from changes in protein structure.

By contrast, the effect of consecutive I172A and L232A mutations on $\Delta G^{\ddagger}$ for TIM-catalyzed isomerization of GAP depends upon the order of these mutations (Scheme 5B). The single I172A and L232A mutations of wild-type TIM result in 2.7 and 1.0 kcal/mol destabilizations of this transition state, respectively (Scheme 5B), while effects on $\Delta G^{\ddagger}$ of I172A (0.9 kcal/mol) and L232A (−0.9 kcal/mol) point mutations for L232A and I172A *Tbb*TIMs are 1.8 and 1.9 kcal/mol more stabilizing, respectively, than the effects of the same mutations on $\Delta G^{\ddagger}$ for wild-type TIM. These results are consistent with the conclusion that the straightforward effects of I172A and L232A mutations on the kinetic parameters for TIM-catalyzed reactions of the substrate pieces (Scheme 5A) reflect the common rate-determining chemical step for these enzyme-catalyzed reactions, but that the more complex effects of these mutations on the kinetic parameters for reaction of the whole substrate GAP reflect the change from a rate-determining physical step for the reaction catalyzed by wild-type *Tbb*TIM[49] to a rate-determining chemical step for the reaction catalyzed by the I172A/L232A mutant.

We propose that the putative 1.8 kcal/mol stabilization by the L232A mutation of active closed enzyme E_C relative to inactive open form E_O (Scheme 6) is not expressed at the rate-determining step for the L232A TIM-catalyzed reaction of GAP, but that this stabilization contributes to the observed effect of the I172A mutation at L232A TIM and of the L232A mutation at I172A TIM. This hypothesis provides a rationalization for the following observations.

(1) The L232A mutation results in a 1.0 kcal/mol increase in $\Delta G^{\ddagger}$ for wild-type TbbTIM-catalyzed isomerization of GAP. The activation barrier ($\Delta G^{\ddagger}$) for the wild-type TIM-catalyzed isomerization of GAP is approximately equal to the barrier for partly rate-limiting diffusion-controlled formation of the Michaelis complex to GAP [k_d (Scheme 7)].[49] Stabilization of

Scheme 7

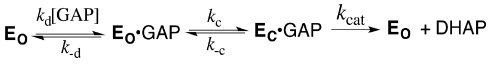

E_C by the L232A mutation cannot result in a large decrease in this barrier to diffusion. We propose that the observed effect of the L232A mutation on $\Delta G^{\ddagger}$ for *Tbb*TIM-catalyzed isomerization of GAP is due to an increase in the barrier to the conformational change that converts E_O·GAP to active E_C·GAP [k_c (Scheme 7)] and that this step is rate-determining for the L232A *Tbb*TIM-catalyzed reaction.

(2) The L232A mutation results in a 0.9 kcal/mol decrease in $\Delta G^{\ddagger}$ for 172A TbbTIM-catalyzed isomerization of GAP. Chemistry [k_{cat} (Scheme 7)] should be cleanly rate-determining for the slow isomerization reaction of GAP catalyzed by I172A *Tbb*TIM. The second L232A mutation results in an 8-fold decrease in K_m and an 8-fold increase in k_{cat}/K_m. This is consistent with an increase in the fraction of enzyme present as E_C, due to stabilization of E_C by the L232A mutation, as discussed above. The L232A mutation now results in a decrease in $\Delta G^{\ddagger}$ for the reactions of the substrate in pieces and the whole substrate, when the height of the reaction barrier to $\Delta G^{\ddagger}$ is controlled by chemistry. The different −1.8 and −0.9 kcal/mol stabilizing effects of the L232A mutation on $\Delta G^{\ddagger}$ for reactions of the substrate in pieces (Scheme 5A) and the whole substrate (Scheme 5B), respectively, might represent some effect of the covalent connection at the whole substrate. For example, independent motion of the pieces GA and HP_i, in the space created by the side chain deletions at the double mutant, could allow access to a reactive binding conformation unavailable to the whole substrate, whose motion is restricted by the covalent connection between the pieces.

(3) The effect of the I172A mutation on $\Delta G^{\ddagger}$ for isomerization of GAP catalyzed by L232A *Tbb*TIM is 1.8 kcal/mol smaller than the effect of this mutation on $\Delta G^{\ddagger}$ for the wild-type *Tbb*TIM-catalyzed reaction. We propose that (1) the 2.7 kcal/mol effect of the I172A mutation on $\Delta G^{\ddagger}$ for wild-type *Tbb*TIM-catalyzed isomerization is close to the intrinsic effect of the mutation on the chemical reaction barrier, (2) the rate constant for the enzyme conformational change, k_c (Scheme 7), which converts E_O·GAP to active E_C·GAP, is rate-determining for isomerization catalyzed by the Leu232 mutant, and (3) the ∼2.7 kcal/mol effect of the I172A mutation on the chemical reaction barrier is attenuated, because the barrier to the chemical step must first be increased to that for the rate-determining conformational change, before there can be an increase in the overall activation barrier ($\Delta G^{\ddagger}$).

Finally, we note that the L232A mutations in wild-type TIM or I172A TIM each result in similar 1.8−1.9 kcal/mol decreases in the activation barrier ($\Delta G^{\ddagger}$) for the third-order reaction of the substrate pieces, with rate constant $(k_{cat}/K_m)_{E\cdot HP_i}/K_d$. However, the effect of the mutation of wild-type *Tbb*TIM is expressed mainly as a decrease in K_d for the binding of phosphite dianion, while the effect of the mutation in I172A *Tbb*TIM is expressed mainly as an increase in $(k_{cat}/K_m)_{E\cdot HP_i}$ for deprotonation of [^{13}C]GA by the binary E·HPO_3^{2-} complex (Table 2); therefore, the stabilizing effect of the second mutation is expressed only at the transition state for the enzyme-catalyzed reaction of the pieces. We are unable to provide a rationalization for this result.

Structure−Function Relationships. The position of the Cα backbone trace of wild-type *Tbb*TIM liganded to PGA (PDB entry 4TIM)[50] can essentially be superimposed on the backbones for the PGA complexes with I172A, L232A, and I172A/L232A mutants. The similarity in the structures of these PGA complexes is illustrated in Figure 3A−C, which show superimpositions, in the region of the enzyme active site, of these structures with the 0.83 Å atomic resolution X-ray crystal structure of wild-type TIM from *L. mexicana* (*Lm*TIM) complexed to PGA (PDB entry 1N55).[9] The X-ray crystal structure for wild-type *Lm*TIM shows two conformations for the side chain of the active site base Glu167, and for the ligand PGA, where the basic side chain and the ligand carboxylate interact through hydrogen bonds, with bond lengths of 2.61 and 2.55 Å.[9]

DOI: 10.1021/acs.biochem.6b00311
Biochemistry 2016, 55, 3036−3047

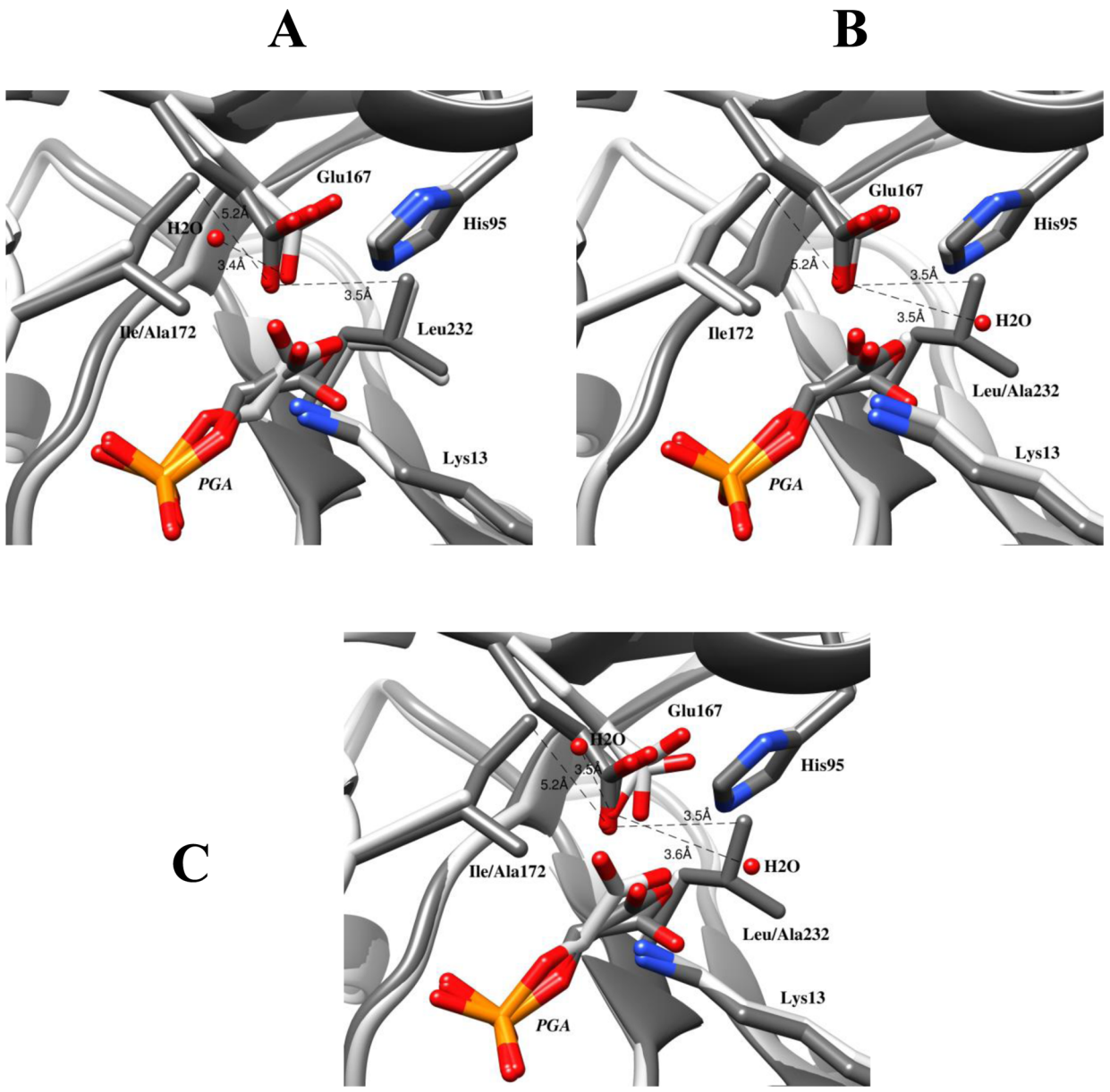

Figure 3. Superimposed crystal structures of the wild-type *Lm*TIM−PGA complex, shown as dark gray ribbons and with atoms colored by element (PDB entry 1N55), and of PGA complexes to mutants of *Tbb*TIM, shown as white ribbons. (A) Subunit A of I172A *Tbb*TIM (PDB entry 5I3I). (B) Subunit B of L232A *Tbb*TIM (PDB entry 5I3K). (C) Subunit B of I172A/L232A *Tbb*TIM (PDB entry 5I3H). These structures show water molecules, which are shown as red spheres, at the site of the excised side chains. The distances of these water molecules from the tip of the hydrophobic side chains and from the basic carboxylate side chain are shown. Weak electron density is observed at the I172A/L232A mutant that is consistent with the presence of a water molecule, but this is not shown in panel C.

Two conformations for the side chain of Glu167 are also observed for the X-ray crystal structure of I172A/L232A *Tbb*TIM.

The neutral imidazole side chain of His95 facilitates carbon deprotonation by stabilizing the transition state negative charge that develops at the enediolate oxygen of the reaction intermediate,[12,13] while the alkylammonium side chain of Lys13 also plays an important electrostatic role in stabilizing negative charge at the enediolate trianion reaction intermediate.[11,33,51,52] The absence of significant changes in the position of these side chains at the mutant *Tbb*TIMs provides strong evidence that the mutations do not affect their functioning in catalysis of the reactions of the whole substrate and substrate pieces. Similarly, I172A and L232A single mutations do not affect the position of the remaining hydrophobic amino acid side chain and therefore are not expected to affect the functioning of this remaining side chain. This is supported by the observation that I172A and L232A mutations in *Tbb*TIM, and the same mutations in *Tbb*TIM previously mutated at the second hydrophobic side chain, result in nearly the same increase in $\Delta G^{\ddagger}$ for catalysis of the reaction of the substrate pieces (Scheme 5A).

The active site for TIM is buried in the protein interior, where it is shielded from interactions with bulk solvent,[21,27] while the side chain of Glu167 has sufficient freedom of motion to conduct proton transfer between C-1 and C-2 of the substrate.[4,53] This is shown in Figure 4A for the X-ray crystal structure of wild-type *Lm*TIM complexed to PGA.[9] Panels B−D of Figure 4 show the corresponding X-ray structures for the complexes of PGA with the I172A, L232A, and I172A/L232A mutants, respectively. Water molecules, represented as red spheres, are within hydrogen bonding distance of the carboxylate side chain

DOI: 10.1021/acs.biochem.6b00311
Biochemistry 2016, 55, 3036−3047

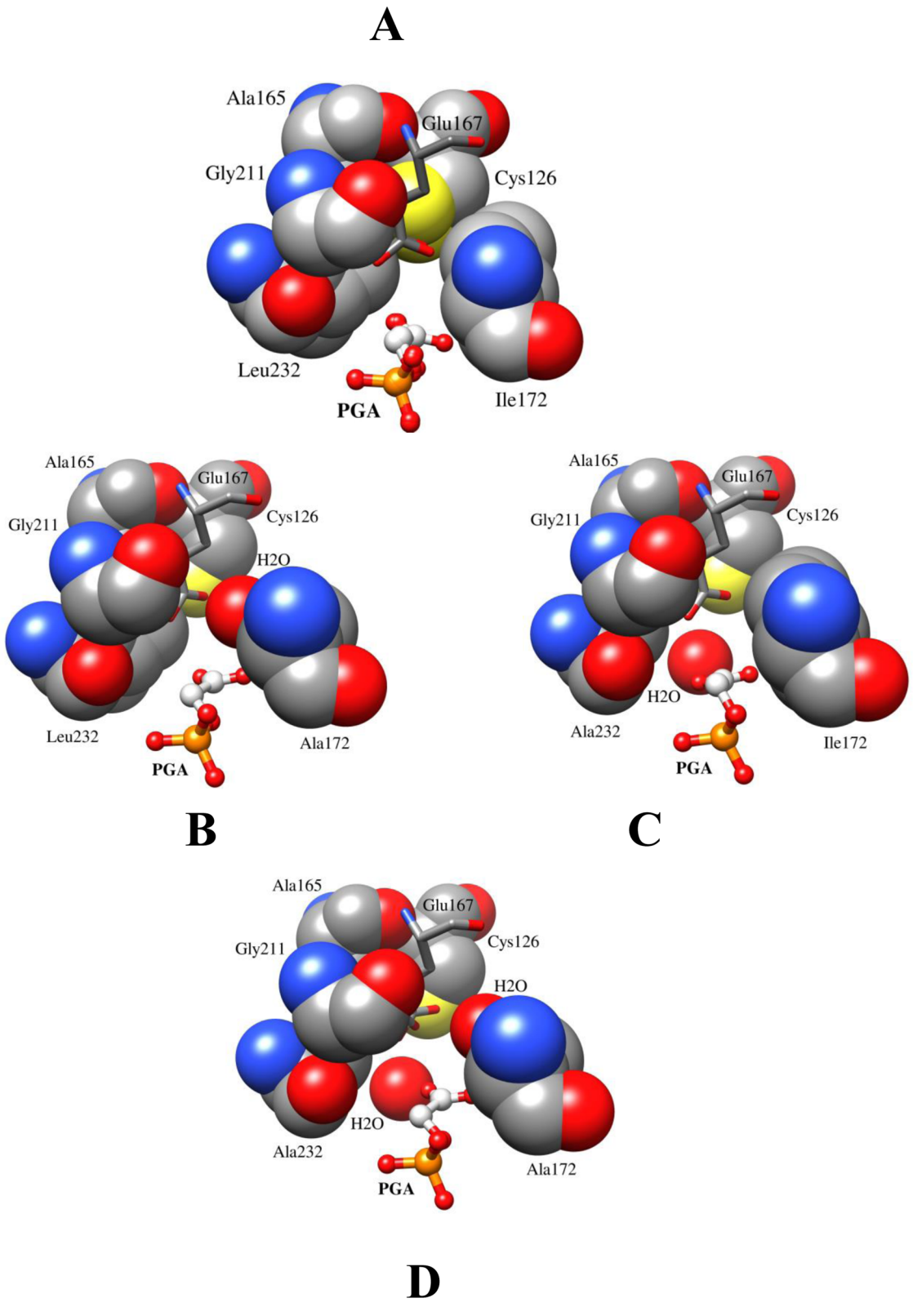

Figure 4. (A) Structure of the closed complex between PGA and wild-type *Lm*TIM PGA (PDB entry 1N55). The side chain of Glu167 sits in a "hydrophobic cage". (B) Structure of the closed complex between PGA and I172A *Tbb*TIM (PDB entry 5I3I). (C) Structure of the closed complex between PGA and L232A *Tbb*TIM (PDB entry 5I3K). (D) Structure of the closed complex between PGA and I172A/L232A *Tbb*TIM (PDB entry 5I3H). Panels B–D show water molecules, located at the site of the excised side chains, as red spheres.

of E167A at the gap created by excision of the hydrophobic side chains. The water at the L232A mutant is sequestered from solvent, while the water at the I172A mutant is connected to the solvent by a water chain.

Water molecules at the active site of TIM were implicated by previous X-ray crystallographic data in the attenuation of the reactivity of the active site carboxylate at the E165D mutant of TIM from chicken muscle (*c*TIM).[54] The E165D mutation of

DOI: 10.1021/acs.biochem.6b00311
Biochemistry 2016, 55, 3036–3047

*c*TIM results in a 140-fold decrease in k_{cat}/K_m for isomerization of GAP, from 7.5×10^6 to 5.4×10^4 M^{-1} s^{-1}, but the k_{cat}/K_m of 1.0×10^6 determined for catalysis by the S96P/E165D double mutant shows recovery of a large fraction of this enzymatic activity.[55] A comparison of the X-ray crystal structures for the complexes of wild-type, E165D, and S96P/E165D TIM to phosphoglycolohydroxamate (PGH) showed only two significant structural changes.[54] (1) The carboxylate side chain at the E165D and S96P/E165D mutants is ~0.7 Å more distant from the PGH ligand than for wild-type TIM. (2) The S96P mutation of E165D TIM results in the displacement of two water molecules from the side chain carboxylate of Asp165 by the side chain of Pro96. This desolvation of the active site carboxylate, and the presumed increase in side chain basicity, results in a k_{cat}/K_m for S96P/E165D 20-fold larger than those of E165D mutant TIMs.

The substitution of water molecules for the excised hydrophobic side chains at I172A and L232A provides a straightforward rationalization for the observed effects of the I172A, but not for the effects of L232A mutations (Tables 1 and 2).

I172A *Tbb*TIM. The I172A mutation results in ~200-fold decreases in the second- and third-order rate constants for deprotonation of the whole substrate and substrate pieces GA and HP_i, respectively (Tables 1 and 2).[28] We have shown that interactions between the hydrophobic side chain of Ile172 and the basic side chain of Glu167 result in an ~2 unit increase in the side chain pK_a of the *Tbb*TIM·PGA complex and have proposed that this increase in basicity promotes efficient catalysis of deprotonation of carbon acid substrates.[20] Figure 3A suggests that these changes in rate and equilibrium constants represent mainly or entirely the effect of replacement of the hydrophobic side chain of Ile172 with the truncated Ala172 side chain and a hydrophilic water molecule. This emphasizes the importance of the hydrophobic side chain in excluding water from the enzyme active site, to enhance the basicity of the carboxylate side chain of Glu167.

L232A *Tbb*TIM. The L232A mutation results in an unexpected 17-fold increase in the second-order rate constant $[(k_{cat}/K_m)_E]$ for the *Tbb*TIM-catalyzed proton transfer reactions of the substrate piece GA in D_2O, a 25-fold increase in the third-order rate constant $[(k_{cat}/K_m)_{E\cdot HP_i}/K_d]$ for reaction of the substrate pieces, and a 16-fold decrease in K_d for binding of HPO_3^{2-} (Scheme 6).[28,29] We proposed that these changes reflect the low concentration of a catalytically active loop-closed form of wild-type TIM [E_C; $K_C \ll 1.0$ (Scheme 6)] and an ~1.7 kcal/mol stabilization of E_C relative to E_O at the L232A mutant. The representations of the crystal structures for the L232A mutants of *Tbb*TIM (Figures 3B and 4C) show a water molecule in the position of the excised hydrophobic side chain. This snapshot serves as a starting point for developing a structure-based explanation of the effect of this mutation on enzyme activity but fails to provide support for the kinetic model shown in Scheme 6. In fact, the replacement waters at the I172A and L232A mutants each lie 3.5 Å from the active site carboxylate and might be expected to cause a similar decrease in side chain reactivity, which is not observed.

We conclude that the X-ray crystal structures for the complexes of PGA to the L232A and I172A/L232A mutants fail to provide a rationalization for the effect of L232A mutations on the reactions of the substrate pieces. We suggest that these structures may not capture the critical effects of this mutation that are responsible for the proposed 20-fold larger value of K_C for the L232A mutant compared with wild-type TIM.

(1) There are important differences in the structures of the TIM·PGA and TIM·DHAP complexes. Inspection of the complex between yeast TIM and DHAP (PDB entry 1NEY)[56] shows a severe steric clash between the bound three-carbon ligand and a water molecule inserted at the same position as in the crystal structure for L232A *Tbb*TIM. We propose that this steric clash exists at the L232A·DHAP complex and forces the putative water out of hydrogen bonding distance with the carboxylate side chain of the catalytic Glu167. (2) The L232A mutation might relieve a small ≤1.7 kcal/mol destabilizing steric interaction between the Leu232 side chain and the protein, which is created during the conversion of E_O to E_C. This barrier may be difficult to identify by inspection of the structures of wild-type TIM.

SUMMARY AND CONCLUSIONS

TIM is more than the collection of catalytic side chains that participate in the chemical isomerization reaction. These side chains are activated for catalysis at the enzyme active site compared to water, and there is no general agreement about the mechanisms for this activation of TIM and other enzymes.[5,6,15,21,27] The ligand-driven conformational change of TIM places the carboxylate side chain of Glu167 in a clamp, which consists of the hydrophobic side chains of Ile172 and Leu232.[9] There is evidence that Ile172 functions to enhance the reactivity of TIM by placing the carboxylate side chain in a hydrophobic environment that enhances side chain basicity.[20]

By contrast, the side chain of Leu232 plays an important role in optimizing the activation of TIM by dianions, by deferring the expression of the dianion binding energy from the Michaelis complex (K_m effect) to the transition state for deprotonation of enzyme-bound carbon acid substrates (k_{cat} effect). Richard and Malabanan proposed that this side chain plays a role in increasing the barrier to the dianion-driven conformational change from E_O to E_C.[28,29] A comparison of the X-ray crystal structures of the complexes of PGA with wild-type, I172A, and L232A *Tbb*TIMs shows that the only significant effect of these mutations is to admit water molecules at the position of the excised side chains, and near the basic side chain of Glu167. These waters provide a simple rationalization for the decreased catalytic activity observed for the I172A mutant, but not for the complex effects of L232A mutations. Our results emphasize on one hand the importance of protein-bound waters in catalysis by TIM but on the other the difficulties in precisely defining their effects on the stability of the rate-determining transition states for reactions catalyzed by TIM mutants.[54,57] We speculate that the failure to fully appreciate the consequences of shifts in the position of enzyme-bound waters has slowed progress toward the development of structure-based rationalization of the effect of mutations at the enzyme active site on enzyme activity.

We propose that the structure-based explanation of the function of the side chain of Leu232 in catalysis might be revealed only by an atomic level X-ray crystal structure for the Michaelis complex of DHAP, and possibly other ligands, with the L232A mutant. These structures would serve as the starting point for high-level computational studies to model the effect of the L232A mutation on the thermodynamic barrier for the activating conformational change in TIM.

ASSOCIATED CONTENT

Supporting Information

The Supporting Information is available free of charge on the ACS Publications website at DOI: 10.1021/acs.biochem.6b00311.

DOI: 10.1021/acs.biochem.6b00311
Biochemistry 2016, 55, 3036−3047

Second-order rate constants and fractional product yields from reactions of the carbonyl form of [1-^{13}C]-GA catalyzed by I172A/L232A *Tbb*TIM in D_2O (Table S1), conditions for the crystallization of TIM mutants (Table S2), diffraction statistics from collection of X-ray data for TIM mutants (Table S3), refinement statistics for TIM mutants (Table S4), and conformational states and occupancy of subunits in the unit cell of crystalline forms of mutants of *Tbb*TIM (Table S5) (PDF)

AUTHOR INFORMATION

Corresponding Author

*Department of Chemistry, University at Buffalo, SUNY, Buffalo, NY 14260. Telephone: (716) 645-4232. Fax: (716) 645-6963. E-mail: jrichard@buffalo.edu.

Funding

This work was supported by the following grants from the National Institutes of Health: GM116921 and GM039754 to J.P.R. and GM116957 to A.M.G. R.K.W. gratefully acknowledges the use of the facilities and expertise of the Biocenter Oulu core facility, a member of Biocenter Finland and Instruct-FI.

Notes

The authors declare no competing financial interest.

ABBREVIATIONS

TIM, triosephosphate isomerase; *Tbb*TIM, TIM from *T. brucei brucei*; *c*TIM, TIM from chicken muscle; *Lm*TIM, TIM from *L. mexicana*; DHAP, dihydroxyacetone phosphate; GAP, (*R*)-glyceraldehyde 3-phosphate; TEA, triethanolamine; GA, glycolaldehyde; PGA, 2-phosphoglycolate; HP_i, phosphite dianion; PGH, phosphoglycolohydroxamate; NADH, nicotinamide adenine dinucleotide, reduced form; NAD^+, nicotinamide adenine dinucleotide, oxidized form; NMR, nuclear magnetic resonance; PDB, Protein Data Bank.

ADDITIONAL NOTE

[a]We note the following small differences in the numbering of amino acid residues of TIM from sources such as yeast and chicken muscle (*c*TIM) and from *Trypanosoma brucei brucei* (*Tbb*TIM) (*c*TIM/*Tbb*TIM): Glu165/Glu167, Pro166/Pro168, Ile170/Ile172, Tyr208/Tyr210, Ser211/Ser213, and Leu230/Leu232.

REFERENCES

(1) Knowles, J. R. (1991) To build an enzyme. *Philos. Trans. R. Soc., B 332*, 115−121.

(2) Knowles, J. R. (1991) Enzyme catalysis: not different, just better. *Nature (London, U. K.) 350*, 121−124.

(3) Knowles, J. R., and Albery, W. J. (1977) Perfection in enzyme catalysis: the energetics of triosephosphate isomerase. *Acc. Chem. Res. 10*, 105−111.

(4) Wierenga, R. K., Kapetaniou, E. G., and Venkatesan, R. (2010) Triosephosphate isomerase: a highly evolved biocatalyst. *Cell. Mol. Life Sci. 67*, 3961−3982.

(5) Richard, J. P. (2012) A Paradigm for Enzyme-Catalyzed Proton Transfer at Carbon: Triosephosphate Isomerase. *Biochemistry 51*, 2652−2661.

(6) Richard, J. P., Zhai, X., and Malabanan, M. M. (2014) Reflections on the catalytic power of a TIM-barrel. *Bioorg. Chem. 57*, 206−212.

(7) Waley, S. G., Miller, J. C., Rose, I. A., and O'Connell, E. L. (1970) Identification of site in triose phosphate isomerase labeled by glycidol phosphate. *Nature (London, U. K.) 227*, 181.

(8) De la Mare, S., Coulson, A. F. W., Knowles, J. R., Priddle, J. D., and Offord, R. E. (1972) Active-site labeling of triose phosphate isomerase. Reaction of bromohydroxyacetone phosphate with a unique glutamic acid residue and the migration of the label to tyrosine. *Biochem. J. 129*, 321−331.

(9) Kursula, I., and Wierenga, R. K. (2003) Crystal structure of triosephosphate isomerase complexed with 2-phosphoglycolate at 0.83-Å resolution. *J. Biol. Chem. 278*, 9544−9551.

(10) Straus, D., Raines, R., Kawashima, E., Knowles, J. R., and Gilbert, W. (1985) Active site of triosephosphate isomerase: in vitro mutagenesis and characterization of an altered enzyme. *Proc. Natl. Acad. Sci. U. S. A. 82*, 2272−2276.

(11) Lodi, P. J., Chang, L. C., Knowles, J. R., and Komives, E. A. (1994) Triosephosphate isomerase requires a positively charged active site: The role of lysine-12. *Biochemistry 33*, 2809−2814.

(12) Komives, E. A., Chang, L. C., Lolis, E., Tilton, R. F., Petsko, G. A., and Knowles, J. R. (1991) Electrophilic catalysis in triosephosphate isomerase: the role of histidine-95. *Biochemistry 30*, 3011−3019.

(13) Nickbarg, E. B., Davenport, R. C., Petsko, G. A., and Knowles, J. R. (1988) Triosephosphate isomerase: removal of a putatively electrophilic histidine residue results in a subtle change in catalytic mechanism. *Biochemistry 27*, 5948−5960.

(14) Richard, J. P. (1984) Acid-base catalysis of the elimination and isomerization reactions of triose phosphates. *J. Am. Chem. Soc. 106*, 4926−4936.

(15) Zhai, X., Malabanan, M. M., Amyes, T. L., and Richard, J. P. (2014) Mechanistic imperatives for deprotonation of carbon catalyzed by triosephosphate isomerase: Enzyme activation by phosphite dianion. *J. Phys. Org. Chem. 27*, 269−276.

(16) Richard, J. P., Amyes, T. L., and Toteva, M. M. (2001) Formation and Stability of Carbocations and Carbanions in Water and Intrinsic Barriers to Their Reactions. *Acc. Chem. Res. 34*, 981−988.

(17) Richard, J. P., and Amyes, T. L. (2001) Proton transfer at carbon. *Curr. Opin. Chem. Biol. 5*, 626−633.

(18) Amyes, T. L., and Richard, J. P. (1996) Determination of the pK_a of ethyl acetate: Brønsted correlation for deprotonation of a simple oxygen ester in aqueous solution. *J. Am. Chem. Soc. 118*, 3129−3141.

(19) Gerlt, J. A., and Gassman, P. G. (1993) Understanding the rates of certain enzyme-catalyzed reactions: Proton abstraction from carbon acids, acyl transfer reactions, and displacement reactions of phosphodiesters. *Biochemistry 32*, 11943−11952.

(20) Malabanan, M. M., Nitsch-Velasquez, L., Amyes, T. L., and Richard, J. P. (2013) Magnitude and origin of the enhanced basicity of the catalytic glutamate of triosephosphate isomerase. *J. Am. Chem. Soc. 135*, 5978−5981.

(21) Richard, J. P., Amyes, T. L., Goryanova, B., and Zhai, X. (2014) Enzyme architecture: on the importance of being in a protein cage. *Curr. Opin. Chem. Biol. 21*, 1−10.

(22) Campbell, I. D., Jones, R. B., Kiener, P. A., Richards, E., Waley, S. C., and Wolfenden, R. (1978) The form of 2-phosphoglycollc acid bound by triosephosphate isomerase. *Biochem. Biophys. Res. Commun. 83*, 347−352.

(23) Hartman, F. C., LaMuraglia, G. M., Tomozawa, Y., and Wolfenden, R. (1975) The influence of pH on the interaction of inhibitors with triosephosphate isomerase and determination of the pK_a of the active-site carboxyl group. *Biochemistry 14*, 5274−5279.

(24) Pompliano, D. L., Peyman, A., and Knowles, J. R. (1990) Stabilization of a reaction intermediate as a catalytic device: definition of the functional role of the flexible loop in triosephosphate isomerase. *Biochemistry 29*, 3186−3194.

(25) Sampson, N. S., and Knowles, J. R. (1992) Segmental movement: definition of the structural requirements for loop closure in catalysis by triosephosphate isomerase. *Biochemistry 31*, 8482−8487.

(26) Zhai, X., Amyes, T. L., and Richard, J. P. (2015) Role of Loop-Clamping Side Chains in Catalysis by Triosephosphate Isomerase. *J. Am. Chem. Soc. 137*, 15185−15197.

DOI: 10.1021/acs.biochem.6b00311
Biochemistry 2016, 55, 3036−3047

(27) Malabanan, M. M., Amyes, T. L., and Richard, J. P. (2010) A role for flexible loops in enzyme catalysis. *Curr. Opin. Struct. Biol. 20*, 702−710.
(28) Malabanan, M. M., Koudelka, A. P., Amyes, T. L., and Richard, J. P. (2012) Mechanism for Activation of Triosephosphate Isomerase by Phosphite Dianion: The Role of a Hydrophobic Clamp. *J. Am. Chem. Soc. 134*, 10286−10298.
(29) Malabanan, M. M., Amyes, T. L., and Richard, J. P. (2011) Mechanism for Activation of Triosephosphate Isomerase by Phosphite Dianion: The Role of a Ligand-Driven Conformational Change. *J. Am. Chem. Soc. 133*, 16428−16431.
(30) Go, M. K., Amyes, T. L., and Richard, J. P. (2009) Hydron Transfer Catalyzed by Triosephosphate Isomerase. Products of the Direct and Phosphite-Activated Isomerization of [1-^{13}C]-Glycolaldehyde in D_2O. *Biochemistry 48*, 5769−5778.
(31) Amyes, T. L., and Richard, J. P. (2007) Enzymatic catalysis of proton transfer at carbon: Activation of triosephosphate isomerase by phosphite dianion. *Biochemistry 46*, 5841−5854.
(32) Malabanan, M. M., Go, M., Amyes, T. L., and Richard, J. P. (2011) Wildtype and Engineered Monomeric Triosephosphate Isomerase from *Trypanosoma brucei*: Partitioning of Reaction Intermediates in D_2O and Activation by Phosphite Dianion. *Biochemistry 50*, 5767−5679.
(33) Go, M. K., Koudelka, A., Amyes, T. L., and Richard, J. P. (2010) Role of Lys-12 in Catalysis by Triosephosphate Isomerase: A Two-Part Substrate Approach. *Biochemistry 49*, 5377−5389.
(34) Borchert, T. V., Pratt, K., Zeelen, J. P., Callens, M., Noble, M. E. M., Opperdoes, F. R., Michels, P. A. M., and Wierenga, R. K. (1993) Overexpression of *trypanosomal* triosephosphate isomerase in Escherichia coli and characterization of a dimer-interface mutant. *Eur. J. Biochem. 211*, 703−710.
(35) Gasteiger, E., Gattiker, A., Hoogland, C., Ivanyi, I., Appel, R. D., and Bairoch, A. (2003) ExPASy: the proteomics server for in-depth protein knowledge and analysis. *Nucleic Acids Res. 31*, 3784−3788.
(36) Gasteiger, E., Hoogland, C., Gattiker, A., Duvaud, S., Wilkins, M. R., Appel, R. D., and Bairoch, A. (2005) Protein identification and analysis tools on the ExPASy server. *Proteomics Protocol Handbook*, 571−607.
(37) Lambeir, A. M., Opperdoes, F. R., and Wierenga, R. K. (1987) Kinetic properties of triose-phosphate isomerase from *Trypanosoma brucei brucei*. A comparison with the rabbit muscle and yeast enzymes. *Eur. J. Biochem. 168*, 69−74.
(38) Amyes, T. L., and Richard, J. P. (1992) Generation and stability of a simple thiol ester enolate in aqueous solution. *J. Am. Chem. Soc. 114*, 10297−10302.
(39) O'Donoghue, A. C., Amyes, T. L., and Richard, J. P. (2005) Hydron Transfer Catalyzed by Triosephosphate Isomerase. Products of Isomerization of (R)-Glyceraldehyde 3-Phosphate in D_2O. *Biochemistry 44*, 2610−2621.
(40) Battye, T. G., Kontogiannis, L., Johnson, O., Powell, H. R., and Leslie, A. G. (2011) iMOSFLM: a new graphical interface for diffraction-image processing with MOSFLM. *Acta Crystallogr., Sect. D: Biol. Crystallogr. 67*, 271−281.
(41) Otwinowski, Z., and Minor, W. (1997) Processing of X-ray Diffraction Data Collected in Oscillation Mode. *Methods Enzymol. 276*, 307−326.
(42) Vagin, A., and Teplyakov, A. (1997) MOLREP: an automated program for molecular replacement. *J. Appl. Crystallogr. 30*, 1022−1025.
(43) Emsley, P., and Cowtan, K. (2004) Coot: model-building tools for molecular graphics. *Acta Crystallogr., Sect. D: Biol. Crystallogr. 60*, 2126−2132.
(44) Murshudov, G. N., Skubak, P., Lebedev, A. A., Pannu, N. S., Steiner, R. A., Nicholls, R. A., Winn, M. D., Long, F., and Vagin, A. A. (2011) REFMAC5 for the refinement of macromolecular crystal structures. *Acta Crystallogr., Sect. D: Biol. Crystallogr. 67*, 355−367.
(45) Adams, P. D., Afonine, P. V., Bunkoczi, G., Chen, V. B., Davis, I. W., Echols, N., Headd, J. J., Hung, L. W., Kapral, G. J., Grosse-Kunstleve, R. W., McCoy, A. J., Moriarty, N. W., Oeffner, R., Read, R. J., Richardson, D. C., Richardson, J. S., Terwilliger, T. C., and Zwart, P. H. (2010) PHENIX: a comprehensive Python-based system for macromolecular structure solution. *Acta Crystallogr., Sect. D: Biol. Crystallogr. 66*, 213−221.
(46) Go, M. K., Malabanan, M. M., Amyes, T. L., and Richard, J. P. (2010) Bovine Serum Albumin-Catalyzed Deprotonation of [1-^{13}C]-Glycolaldehyde: Protein Reactivity toward Deprotonation of the α-Hydroxy α-Carbonyl Carbon. *Biochemistry 49*, 7704−7708.
(47) Alber, T., Banner, D. W., Bloomer, A. C., Petsko, G. A., Phillips, D., Rivers, P. S., and Wilson, I. A. (1981) On the three-dimensional structure and catalytic mechanism of triose phosphate isomerase. *Philos. Trans. R. Soc., B 293*, 159−171.
(48) Sampson, N. S., and Knowles, J. R. (1992) Segmental motion in catalysis: investigation of a hydrogen bond critical for loop closure in the reaction of triosephosphate isomerase. *Biochemistry 31*, 8488−8494.
(49) Blacklow, S. C., Raines, R. T., Lim, W. A., Zamore, P. D., and Knowles, J. R. (1988) Triosephosphate isomerase catalysis is diffusion controlled. *Biochemistry 27*, 1158−1165.
(50) Noble, M. E., Verlinde, C. L., Groendijk, H., Kalk, K. H., Wierenga, R. K., and Hol, W. G. (1991) Crystallographic and molecular modeling studies on *trypanosomal* triosephosphate isomerase: a critical assessment of the predicted and observed structures of the complex with 2-phosphoglycerate. *J. Med. Chem. 34*, 2709−2018.
(51) Joseph-McCarthy, D., Lolis, E., Komives, E. A., and Petsko, G. A. (1994) Crystal structure of the K12M/G15A triosephosphate isomerase double mutant and electrostatic analysis of the active site. *Biochemistry 33*, 2815−2823.
(52) Go, M. K., Amyes, T. L., and Richard, J. P. (2010) Rescue of K12G mutant TIM by NH_4^+ and alkylammonium cations: The reaction of an enzyme in pieces. *J. Am. Chem. Soc. 132*, 13525−13532.
(53) Alahuhta, M., and Wierenga, R. K. (2010) Atomic Resolution crystallography of a complex of triosephosphate isomerase with a reaction intermediate analog: new insight in the proton transfer reaction mechanism. *Proteins: Struct., Funct., Genet. 78*, 1878−1888.
(54) Komives, E. A., Lougheed, J. C., Liu, K., Sugio, S., Zhang, Z., Petsko, G. A., and Ringe, D. (1995) The Structural Basis for Pseudoreversion of the E165D Lesion by the Secondary S96P Mutation in Triosephosphate Isomerase Depends on the Positions of Active Site Water Molecules. *Biochemistry 34*, 13612−13621.
(55) Blacklow, S. C., Liu, K. D., and Knowles, J. R. (1991) Stepwise improvements in catalytic effectiveness: independence and interdependence in combinations of point mutations of a sluggish triosephosphate isomerase. *Biochemistry 30*, 8470−8476.
(56) Jogl, G., Rozovsky, S., McDermott, A. E., and Tong, L. (2003) Optimal alignment for enzymatic proton transfer: structure of the Michaelis complex of triosephosphate isomerase at 1.2-Å resolution. *Proc. Natl. Acad. Sci. U. S. A. 100*, 50−55.
(57) Zhang, Z., Komives, E. A., Sugio, S., Blacklow, S. C., Narayana, N., Xuong, N. H., Stock, A. M., Petsko, G. A., and Ringe, D. (1999) The Role of Water in the Catalytic Efficiency of Triosephosphate Isomerase. *Biochemistry 38*, 4389−4397.
(58) Trentham, D. R., McMurray, C. H., and Pogson, C. I. (1969) The active chemical state of D-glyceraldehyde 3-phosphate in its reactions with D-glyceraldehyde 3-phosphate dehydrogenase, aldolase and triose phosphate isomerase. *Biochem. J. 114*, 19−24.
(59) Albery, W. J., and Knowles, J. R. (1976) Free-energy profile for the reaction catalyzed by triosephosphate isomerase. *Biochemistry 15*, 5627−5631.

DOI: 10.1021/acs.biochem.6b00311
Biochemistry 2016, 55, 3036−3047